Plasma pressure broadening for few-electron emitters including strong electron collisions within a quantum-statistical theory

Sonja Lorenzen* and Banaz Omar
Institute of Physics, University of Rostock, D-18051 Rostock, Germany

Mark C. Zammit, Dmitry V. Fursa, and Igor Bray
Institute of Theoretical Physics, Curtin University, Perth, Western Australia 6845, Australia

(Received 15 May 2013; revised manuscript received 18 December 2013; published 21 February 2014)

To apply spectroscopy as a diagnostic tool for dense plasmas, a theoretical approach to pressure broadening is indispensable. Here, a quantum-statistical theory is used to calculate spectral line shapes of few-electron atoms. Ionic perturbers are treated quasistatically as well as dynamically via a frequency fluctuation model. Electronic perturbers are treated in the impact approximation. Strong electron-emitter collisions are consistently taken into account with an effective two-particle T-matrix approach. Convergent close-coupling calculations give scattering amplitudes including Debye screening for neutral emitters. For charged emitters, the effect of plasma screening is estimated. The electron densities considered reach up to $n_e = 10^{27}$ m^{-3}. Temperatures are between $T = 10^4$ and 10^5 K. The results are compared with a dynamically screened Born approximation for Lyman lines of H and H-like Li as well as for the He 3889 Å line. For the last, a comprehensive comparison to simulations and experiments is given. For the H Lyman-α line, the width and shift are drastically reduced by the Debye screening. In the T-matrix approach, the line shape is notably changed due to the dependence on the magnetic quantum number of the emitter, whereas the difference between spin-scattering channels is negligible.

DOI: 10.1103/PhysRevE.89.023106 PACS number(s): 52.25.Os, 32.70.Jz, 34.80.Bm

I. INTRODUCTION

Plasma pressure broadening (PPB), i.e., broadening and shift of spectral lines due to the plasma surroundings, has been studied for a long time. In particular, it can be used for plasma diagnostics, as reviewed, e.g., in [1]. The charged plasma particles affect the atomic states of the emitting atom or ion. The mechanisms are the same, no matter if the plasma is part of an astrophysical object or created in the laboratory, e.g., in arc discharges or by laser impact. A sound theory to calculate line profiles is needed in order to obtain accurate information about plasma parameters such as composition, temperature, and density from the measured line spectrum. Several approaches are applied to calculate the spectrum of bound-bound electron transitions, emitted from or absorbed by a plasma. Some use pure quantum mechanics [2], others involve a semiclassical view of the perturbers, e.g., the standard theory [3,4], or they depend on molecular dynamics (MD) simulations, e.g., [5].

All theories are based on the calculation of the dipole-dipole correlation function, which describes the emission or absorption of radiation from charged particles. Within our quantum-statistical theory, the dipole-dipole correlation, i.e., the polarization function, is calculated with the help of thermodynamic Green's functions; see [6–8]. For dense plasmas, strong electron-emitter collisions are important and perturbative methods are no longer applicable. One way to include strong collisions in the framework of the standard theory has been discussed in Ref. [9], allowing for penetrating collisions.

The aim of this work is to treat strong electron-emitter collisions consistently within quantum-statistical theory. For this reason, we combine sophisticated scattering theory with our line shape formalism; thus, we go beyond the perturbative Born approximation. We show that plasma screening has to be included in the scattering process, otherwise the line shift and width are overestimated. Furthermore, we discuss the resulting line shapes, when different spin-scattering channels and emitter states with different magnetic quantum numbers are considered separately.

The theory is briefly reviewed in Sec. II with a focus on the treatment of strong electron-emitter collisions. They can be included by ladderlike diagrams in our theory. Neglecting the dynamical screening, an effective two-particle T-matrix approach can be derived; see [10]. Then, the electronic contribution to PPB is given by the electron-emitter scattering amplitude. It is obtained from convergent close-coupling (CCC) calculations for electron scattering on a Debye-screened neutral emitter; see [11,12]. Hence, we go beyond the close-coupling approach presented by Unnikrishnan and Callaway [13] which does not include screening. In our theory, electron scattering on charged emitters in a plasma surrounding is approximated by isolated electron-emitter scattering [14–16]. We show in Appendix A that the divergent Coulomb part of the scattering amplitudes can be removed. We estimate the error made by neglecting the screening in Appendix B. PPB by perturbing ions is treated quasistatically or dynamically using the renewed formulation of the frequency fluctuation model (FFM) [17].

Our first example is the H Lyman-α (L_α) line in Sec. III. Its simplicity makes it an ideal test case; however, its shape has recently been discussed controversially at the spectral line shapes in plasmas code comparison workshop [18]. For H L_α, we compare the PPB of electrons in the effective T-matrix approach with and without Debye screening to a dynamically screened Born approximation for $n_e = 10^{25}$ m^{-3} at $T =$ 11 604 K. Furthermore, we give a comparison to the measured H L_α profiles of Grützmacher and Wende [19]. In Sec. IV, we apply the effective T-matrix approach to a charged H-like emitter. Full Lyman line profiles of Li^{2+} are calculated for the free-electron densities of $n_e = 4 \times 10^{25}$ m^{-3} and

*Sonja.L@renzen.de

4×10^{26} m^{-3} at a temperature of $T = 3 \times 10^5$ K. Here, the asymmetry of L_β and L_γ lines is drastically changed when applying the T-matrix approach without screening. Screening corrections are estimated and lead to a better agreement between the two approaches. A comparison of the linewidth from the two approaches is carried out for $n_e = 10^{25}$–10^{27} m^{-3}. The last example on the He 3889 Å line is given in Sec. V. There, results for the linewidth and shift of the T-matrix approach are compared to experimental data, results of computer simulations, and other theories for the density range $n_e = 10^{22}$–10^{24} m^{-3} and $T \sim 10^4$ K

II. QUANTUM-STATISTICAL APPROACH TO PLASMA PRESSURE BROADENING

The quantum-statistical theory for pressure broadening has been described in detail in [6–8]. Here, we give only the key formulas in atomic Rydberg units, i.e., $\hbar = 2m_e = e^2/2 = 1$. These units are used throughout this paper. In the case of local thermodynamic equilibrium, the emitted spectral intensity $I(\Delta\omega)$ at $\Delta\omega = \omega - \omega_0$ near the frequency ω_0 of the unperturbed transition is given by

$$I(\Delta\omega) = \frac{(\omega_0 + \Delta\omega)^4}{8\pi^4 c^3} e^{-(\omega_0+\Delta\omega)/k_\mathrm{B}T} \times \mathrm{Im}\left[\sum_{ii'ff'} \{\langle i|\vec{r}|f\rangle\langle f'|\vec{r}|i'\rangle\langle i|\langle f|U(\Delta\omega)|f'\rangle|i'\rangle\}\right] \tag{1}$$

with the speed of light c and the Boltzmann constant k_B. The sum runs over all initial i and final f emitter states. The double sum is not necessary for isolated lines. The contributions to the line profile are weighted with the transition probability, which is given by the dipole matrix elements $\langle i|\vec{r}|f\rangle$. The time evolution operator $U(\Delta\omega)$ can be taken in different approximations. For the quasistatic approximation, it is given by

$$U(\Delta\omega)_\mathrm{static} = \langle L(\Delta\omega, E)^{-1}\rangle_\mathrm{s} = \int_0^\infty dE\, W(E) L(\Delta\omega, E)^{-1}, \tag{2}$$

where $\langle\cdots\rangle_s$ stands for the average over the static ion microfield with the microfield distribution function $W(E)$. For neutral emitters, i.e., hydrogen and helium, we use Hooper's low-frequency tables [20] to determine $W(E)$ for weakly coupled plasmas. Outside the validity range of Hooper's approach, we use the fit formula of Potekhin *et al.* [21]. The fit formula is based on Monte Carlo simulations and is appropriate for strongly coupled plasmas as well. For the charged H-like emitter Li^{2+}, we use APEX [22] to calculate $W(E)$ with Debye-Hückel pair correlation functions.

The line profile operator $L(\Delta\omega, E)$ contains the width and shift of atomic energy levels caused by the plasma surroundings according to

$$L(\Delta\omega, E) = \Delta\omega - \mathrm{Re}[\Sigma_{ii'}(\Delta\omega) - \Sigma_{ff'}(\Delta\omega)] + \imath\,\mathrm{Im}[\Sigma_{ii'}(\Delta\omega) + \Sigma_{ff'}(\Delta\omega)] + \Gamma_{ii'ff'}(\Delta\omega). \tag{3}$$

Here, $\Sigma_{ii'}$ and $\Sigma_{ff'}$ are the self-energies, i.e., the shift (real part) and broadening (imaginary part), of energy levels i and f due to the surrounding plasma, respectively, and $\Gamma_{ii'ff'}$ is the upper-lower level coupling term. Due to different interaction time scales, the self-energy can be split into a nondiagonal E-field-dependent ionic part and a diagonal frequency-dependent electronic part,

$$\Sigma_{\nu\nu'}(E, \Delta\omega) = \Sigma^i_{\nu\nu'}(E) + \Sigma^e_\nu(\Delta\omega)\delta_{\nu\nu'}, \tag{4}$$

with $\nu = i, f$. Now, we discuss the details of the self-energy calculation for ions and electrons separately.

A. Perturbing ions

The perturbation of the emitter by the plasma ions is mainly caused by the linear and quadratic Stark effects. The linear Stark effect is nonzero for H and H-like emitters and given analytically in parabolic coordinates [23]. For He, the quadratic Stark effect gives the first nonvanishing contribution. The wave functions enter into the calculation for He. As they are not given analytically, we approximate their spherical part by a linear combination of H-like wave functions. The radial part is calculated by the Coulomb approximation after Bates and Damgaard [24]; for more details see [25]. Furthermore, the inhomogeneity of the ionic microfield is treated by the quadrupole Stark effect after Halenka [26], leading to a nondiagonal term in the ionic self-energy $\Sigma^i_{\nu\nu'}(E)$.

For high densities and low temperatures, the ions' movement during the time of emission is negligible and the quasistatic limit can be applied. Then, the time evolution operator is given by Eq. (2). In the opposite regime, ion dynamics has to be treated seriously. There exist several methods to include ion dynamics; for an overview see Refs. [1,27]. In particular, molecular dynamics simulations are a useful tool to treat the dynamics of the system. However, we want to keep the line shape calculations analytic. Recently, a comparison of two analytic methods—the model microfield method (MMM) [28,29] and the FFM [17]—was presented for a broad range of plasma parameters for H Lyman lines [30]. For H L_α, differences between the two approaches up to ±30% were observed for the full width at half maximum (FWHM). As the focus of this communication is on the contribution of strong electron collisions, we present only the FFM briefly here and use it throughout the paper. However, since the use of the MMM leads to a better agreement with the Grützmacher-Wende experiment, we give results for MMM ion dynamics there, too. Details of our implementation of MMM can be found in [30].

The FFM connects microfield fluctuations with frequency fluctuations. It assumes that the emitting system can be described by a set of dressed two-level transitions each with a certain frequency, amplitude, and width [17]. Starting from the area-normalized line profile $I_s(\omega)$ calculated in the quasistatic limit, e.g., with Eqs. (1) and (2), the dynamic profile is given by

$$I_\mathrm{FFM}(\omega) \sim \mathrm{Re}\frac{Q(\omega,\gamma)}{1 - \gamma\, Q(\omega,\gamma)} \tag{5}$$

with

$$Q(\omega,\gamma) = \int_0^\infty \frac{I_s(\omega')d\omega'}{\gamma + \imath(\omega - \omega')}. \quad (6)$$

Here, γ is the inverse state lifetime

$$\gamma = \frac{v_{\text{therm}}}{d_i}. \quad (7)$$

It depends on the thermal velocity of ions $v_{\text{therm}} = \sqrt{8k_BT/(\pi m_i)}$ and the mean ion distance $d_i = [3/(4\pi n_i)]^{1/3}$, where m_i and n_i are the mass and density of the perturbing ions, respectively. For large γ, the high-frequency limit is reproduced and a Lorentzian line shape is obtained. Although the FFM does not reproduce the second moment of the microfield distribution correctly, the resulting line profiles compare well to simulated line shapes [17].

B. Perturbing electrons

In contrast to the ions, the electron dynamics plays a crucial role, and thus the quasistatic approximation is not applicable. Furthermore, multiple electron-emitter collisions occur and have to be treated. Within our quantum-statistical view of spectral line shapes, two approaches have been developed to account for the contribution by free electrons. Perturbing electrons are considered either within a dynamically screened Born approximation (first order) or within an effective two-particle T-matrix approach which can so far take only static (Debye) screening into account.

1. Dynamically screened Born approximation

The self-energy in the Born approximation is given by [6]

$$\Sigma_\nu^e(\Delta\omega) = -\int \frac{d^3q}{(2\pi)^3} V(q) \sum_\alpha \left|M_{\nu\alpha}^0(q)\right|^2 \times \int_{-\infty}^\infty \frac{d\omega}{\pi}[1 + n_B(\omega)] \frac{\text{Im}\,\varepsilon^{-1}(\vec{q},\omega + \imath\,\delta)}{\Delta\omega + \omega_{\nu\alpha} - (\omega + \imath\delta)}. \quad (8)$$

The dielectric function $\varepsilon(\vec{q},\omega + \imath\delta)$ is approximated by the dielectric function in the random phase approximation. $M_{\nu\alpha}^0(q)$ is the vertex contribution for virtual transitions from ν to α. For H and Li^{2+}, we restrict the main quantum number n_α to run from $n_\nu - 1$ to $n_\nu + 2$ for the real part of $\Sigma_\nu^e(\Delta\omega)$. For the imaginary part, we use the no-quenching approximation $n_\alpha = n_\nu$, since it gives the main contribution to the line broadening. For He, n_α runs always from $n_\nu - 2$ to $n_\nu + 2$. $V(q) = Z_{\text{ion}}e^2/\varepsilon_0 q^2$ is the Fourier-transformed Coulomb potential and $n_B(\omega) = \{\exp[\hbar\omega/(k_BT)] - 1\}^{-1}$ is the Bose function. For the evaluation of Eq. (8) we consider the frequency-independent case $\Delta\omega = 0$ which corresponds to the binary collision approximation. This alters the line profile negligibly, e.g., for H L_α at $T = 11\,604$ K and $n_e = 1 \times 10^{25}$ m^{-3}, the resulting FWHM is 1% smaller in test calculations with full $\Delta\omega$ dependence in Eq. (8). For all considered lines, we followed the method in Refs. [31,32] and checked that correlated collisions can be neglected for our plasma parameters.

The coupling contribution—also called the vertex term—is given in a similar way:

$$\Gamma_{ii'ff'} = -\imath \int \frac{d^3q}{(2\pi)^3} M_{i'i}^0(-\vec{q}) M_{f'f}^0(\vec{q}) V(q) \times \int_{-\infty}^\infty d\omega[1 + n_B(\omega)]\text{Im}\,\varepsilon^{-1}(\vec{q},\omega + \imath\delta)\delta(\omega). \quad (9)$$

The correct dynamical screening of weak collisions is included in Eqs. (8) and (9) by the imaginary part of the inverse dielectric function. However, the Born approximation overestimates strong collisions. This can be rectified to some extent by a cutoff $q_{\max} = 1/\rho_{\min}$. For the case of H, $q_{\max,\text{H}}$ has been adjusted in such a way that the self-energies of an advanced T-matrix approach are recovered; see Ref. [33]. For Li^{2+}, we use a cutoff scaled by the square of the atomic number $Z = 3$, i.e.,

$$q_{\max,Z} = Z^2 q_{\max,\text{H}}. \quad (10)$$

Since there are no advanced T-matrix calculations available for He, we follow the cutoff procedure introduced by Griem *et al.* [3,34]. There, the minimum impact parameter $\rho_{\min}$ is calculated under the assumption of straight electron trajectories in order to assure the unitarity of the scattering matrix. Then a strong collision term for the width is added [34],

$$\Delta\Sigma_{\text{strong}}^e \approx 1.21\imath n_e v_{\text{therm}} \pi q_{\max}^{-2}, \quad (11)$$

depending on the free-electron density n_e and the thermal velocity v_{therm} of the electrons. Further details about the evaluation of Eqs. (8) and (9) can be found in Refs. [6–8,25].

2. Effective two-particle T-matrix approximation

The effective T-matrix approach is a reduced version of the T-matrix approach presented in [33]. It can describe weak and strong collisions equally well, but so far only includes static screening [10,35]. For a nondegenerate plasma, the electronic self-energy, again evaluated at $\Delta\omega = 0$, is then given by

$$\Sigma_\nu^e = -\frac{2}{\pi} n_e \Lambda_{\text{th}}^3 \int_0^\infty dk\, k^2 e^{-k^2/k_BT} f_\nu(0,k). \quad (12)$$

Plasma properties enter via the electron density n_e and the thermal wavelength $\Lambda_{\text{th}} = \sqrt{4\pi/k_BT}$ as well as the forward scattering amplitude $f_{i,f}(0,k)$ for elastic electron scattering at the Debye-screened emitter in state i and f, respectively. This expression, Eq. (12), was also found by Baranger in [2]. He uses the impact approximation and treats the perturbing electrons quantum-mechanically. Fluctuating interactions are replaced by a constant effective one-perturber-atom interaction. In Ref. [2], a level coupling term is derived as well, which is given by

$$\Gamma_{if} = \frac{2\imath}{\pi} n_e \Lambda_{\text{th}}^3 \int_0^\infty dk\, k^3 e^{-k^2/k_BT} \times \int_0^\pi d\theta\, \sin(\theta) f_f(\theta,k) f_i^*(\theta,k). \quad (13)$$

Here, θ is the scattering angle and the dependence of the scattering amplitudes on θ has to be known, too.

The scattering amplitudes, which enter Eqs. (12) and (13), are obtained from a convergent close-coupling calculation.

For the neutral emitters (H, He), it is modified to include Debye screening in the interaction potentials. For the charged emitter (Li^{2+}), we neglect screening and estimate the error thus made. Details of the CCC method and its modification can be found in [14–16] and [11,12], respectively. For H and Li^{2+}, we use 54 (Sturmian) Laguerre functions as a basis for bound and continuous emitter states. With this choice, the emitter states up to $4f$ are reproduced with the correct energies. 153 pseudostates are used to describe electron-He scattering; all details can be found in Ref. [12].

The electron-electron interaction is treated within a partial wave decomposition, where the first partial waves (up to 70) are considered directly. For larger numbers of partial waves, scattering amplitudes are extrapolated following O'Malley *et al.*'s approach [36]. The coupled equations are solved in momentum space and lead to the scattering amplitude. Our method gives separate results for singlet and triplet scattering channels as well as for scattering at the emitter with initial and final states $n_i,l_i,m_i \rightarrow n_f,l_f,m_f$. Here, we consider only elastic scattering $n_i,l_i,m_i \rightarrow n_i,l_i,m_i$ to calculate the self-energies and level coupling term.

III. HYDROGEN

The L_α line of hydrogen serves as a testbed. It is emitted in the electron transition from $n = 2$ to the ground state $1s$. First, we study the contributions of the electrons for the example of a plasma with Debye screening length $D = \sqrt{k_B T/8\pi n_e} = 44a_0$. This corresponds, e.g., to plasma conditions $T = 11\,604$ K and $n_e = 1 \times 10^{25}$ m^{-3}, where strong electron collisions are relevant due to the high electron density. Then, we reconsider the measured L_α spectra of Grützmacher and Wende [19] with larger screening length $D \sim 300a_0$.

A. Strong collisions and Debye screening

We investigate the influence of screening in the convergent coupling calculation. This has been done in detail for the cross sections σ in [11]. Now, we are explicitly interested in real and imaginary part of the forward scattering amplitude $f(\theta = 0,k)$, as they enter in Eq. (12) and lead to shift (real part) and broadening (imaginary part) of the line. We concentrate on the upper $2p$ states, as the contribution of the lower level $1s$ is small. The effect of screening can be seen in Fig. 1 for the forward scattering amplitude of e-H$(2p,m = \pm 1)$ scattering. The scattering amplitudes are reduced by screening. Thus, the resulting self-energies are reduced, too. As the different spin-scattering channels lead only to slightly different scattering amplitudes in the low-energy region $k < 0.7a_0$, averaging over spin-scattering channels has been carried out. The results for Σ^e_{2p} and $\Gamma_{2p;1s}$ can be found in Table I together with the ones obtained from the dynamically screened Born approximation from Eqs. (8) and (9). The Born approximation gives the same results for different magnetic quantum numbers m. The shift ($\mathrm{Re}[\Sigma^e_{2p}]$) is still overestimated by a factor of 3 even after the cutoff has been applied to account for strong collisions. The width ($\mathrm{Im}[\Sigma^e_{2p}]$) is sufficiently reduced by the cutoff procedure. The width from the Born approximation

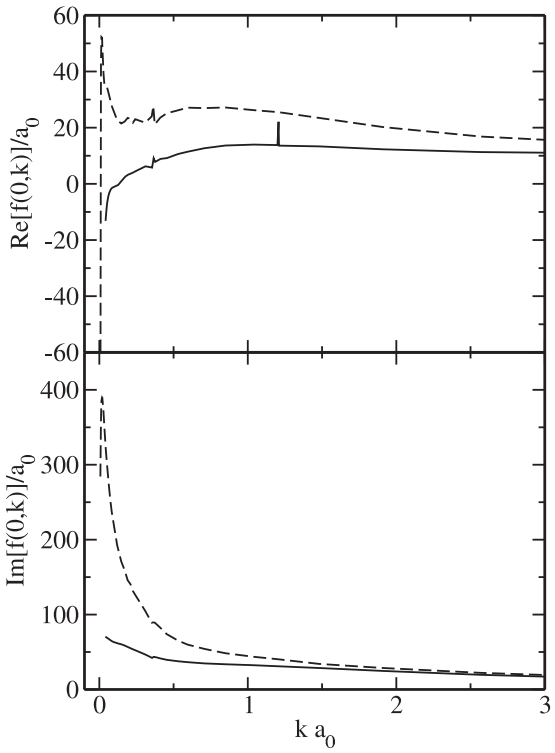

FIG. 1. Forward scattering amplitude for scattering of an electron with momentum k on a H atom in state $2p$ ($m = \pm 1$) without screening (broken line) and with Debye screening for $D = 44a_0$ (full line). Spikes are due to resonances.

TABLE I. Self-energy Σ^e_{2p} from Eqs. (8) and (12) and coupling term $\Gamma_{2p;1s}$ from Eqs. (9) and (13) in different approximations in units of 10^{-4}Ry: The spin-averaged, m-dependent T-matrix approach is given without screening and with Debye screening ($D = 44a_0$) and compared to the m-independent dynamically screened Born approximation with full integration and cutoff at $q_{\max}$, respectively. The considered hydrogen plasma has $n_e = 10^{25}$ m^{-3} at $T = 11\,604$ K.

	T matrix						Born approximation	
	$m = \pm 1$		$m = 0$		m average		$m = 0, \pm 1$	
	Unscreened	$D = 44a_0$	Unscreened	$D = 44a_0$	Unscreened	$D = 44a_0$	Without cutoff	With cutoff
$\mathrm{Re}[\Sigma^e_{2p}]$	− 4.38	− 1.03	− 1.51	0.083	− 3.42	− 0.66	− 9.61	− 3.36
$\mathrm{Im}[\Sigma^e_{2p}]$	− 21.8	− 9.07	− 6.76	− 4.22	− 16.8	− 7.46	− 11.0	− 6.46
$\mathrm{Re}[\Gamma_{2p;1s}]$	0.09	0.11	− 0.05	− 0.05	0.04	0.06	0.0	0.0
$\mathrm{Im}[\Gamma_{2p;1s}]$	0.13	0.13	0.48	0.43	0.25	0.23	0.63	0.24

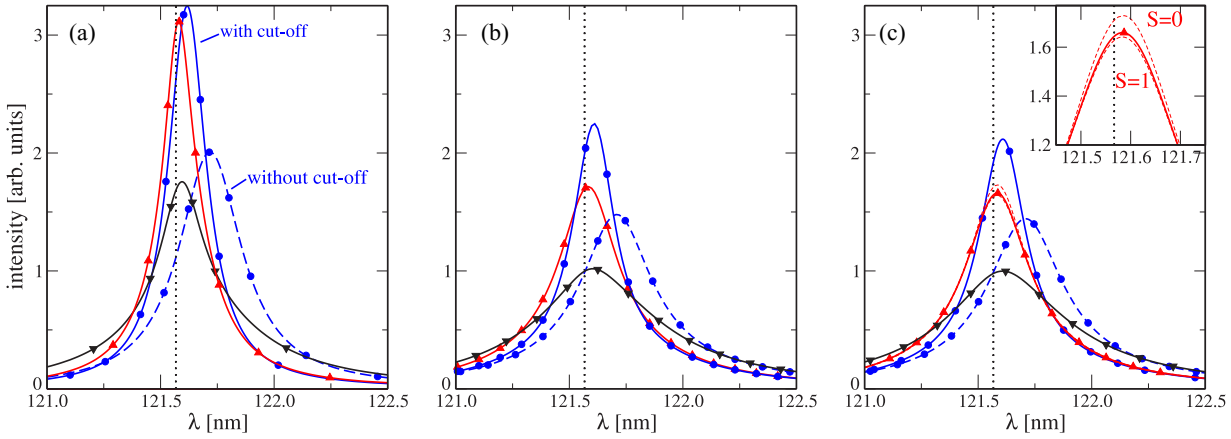

FIG. 2. (Color online) Full H L_α profile calculated in different approximations for $T = 11\,604$ K and $n_e = 10^{25}$ m^{-3}. (a) Only electronic contributions in (●) the dynamically screened Born approximation, (▼) the T-matrix results without screening, and (▲) the T-matrix approach with screening ($D = 44a_0$). (b) Electronic contributions and static ions and (c) electronic contributions and ion dynamics in the FFM. Inset: Different line shapes for pure singlet ($S = 0$) and triplet ($S = 1$) electron-emitter scattering channels (red broken lines). Doppler broadening is included and all profiles are area normalized.

is between the two m-dependent T-matrix results, only 14% below their average.

The resulting L_α line profile of hydrogen is shown in Fig. 2. As long as only electrons are considered [Fig. 2(a)], the widths from the T-matrix approach and in the Born approximation with cutoff are similar, i.e., the cutoff procedure gives a reasonable correction. Nevertheless, the line with ionic Stark splitting [Fig. 2(b)] is broader for the m-dependent T-matrix calculation compared to the m-independent Born approach. This is because the central components ($m = \pm 1$) are broader in the T-matrix approach than the shifted components ($m = 0$, i.e., $2p$ with $2s$ superposed). The approach which can resolve the dependence on the magnetic quantum number m represents the physics of the line emission process better.

In Fig. 2(c), the full treatment including FFM ion dynamics is shown. The ion dynamics lead to further broadening of the line. There, singlet ($S = 0$) and triplet ($S = 1$) electron-emitter scattering channels are considered separately, too. In the inset, this is shown in more detail. Although the line is narrower for $S = 0$ and broader for $S = 1$, their average coincides with the one calculated with spin-averaged electronic self-energies. Hence, it is justified to average over the spin-scattering channels when Eqs. (12) and (13) are evaluated.

B. Grützmacher-Wende experiment reconsidered

In the experiment of Grützmacher and Wende [19], a wall-stabilized argon arc source was used to create dense equilibrium plasmas with $n_e \sim 10^{23}$ m^{-3} at $T \sim 10^4$ K. Under these conditions, pressure broadening by electrons and Ar^+ ions dominates over the Doppler broadening of the L_α line of H. With a hydrogen density of $n_H < 10^{19}$ m^{-3}, the plasma was optically thin and reabsorption could be avoided. The spectrometer bandwidth was stated to be better than $\lambda/\Delta\lambda = 30\,390$. The measured line profiles were already compared to the results of the unified theory in [19], and the remaining discrepancy was resolved by Lee [37] with a perturbative method taking ion dynamics into account. Here, the importance of ion dynamics for L_α was emphasized.

We use the data of Grützmacher and Wende for a comparison, as we are not aware of a better measurement of H L_α under dense plasma conditions. Our theoretical results use singly charged argon ions as perturbers with FFM ion dynamics. To emphasize the importance of ion dynamics, results with MMM ion dynamics are discussed as well. The electronic medium effects are calculated with Eqs. (12) and (13) using scattering amplitudes from unscreened and Debye-screened interactions. We average over the spin-scattering channels and apply a Gaussian instrumental broadening ($\lambda/\Delta\lambda = 30\,390$). The use of the effective T-matrix approach leads to a better agreement with the experimental data than the use of the Born approximation from Eqs. (8) and (9); see Table II. For $n_e = (2,3) \times 10^{23}$ m^{-3}, both the unscreened and screened T-matrix approaches with the MMM agree with the experiment. For the lowest density, only the FWHM without screening lies within the confidence interval of the experiment, in contrast to the highest density, where the screening has to be taken into account to reproduce the experimental FWHM. As has been shown in an earlier paper [30], the FFM leads to narrower lines than the MMM in the considered density and temperature region. Thus, it does not reproduce the experimental linewidth within the framework of our theory. Furthermore, we give the results of Halenka and Olchawa [38] in Table II, who used computer simulations to calculate the L_α lines in full agreement with the experiment.

For $n_e = 2 \times 10^{23}$ m^{-3} and $T = 13\,200$ K, the full Lyman-α line profile is considered,; see Fig. 3. The main contribution to the linewidth is caused by ion dynamics. It is crucial for this experiment, as was already shown in [37]. Nevertheless, the effective T-matrix approach gives a better agreement with the measurement than the Born approach with cutoff procedure. As has been discussed above, the additional broadening is mainly caused by the m dependence of the electronic self-energy in the effective T-matrix approach.

TABLE II. FWHM of H L_α in Å for the experimental conditions of Grützmacher and Wende [19]: Comparison of the m-dependent T-matrix approach (averaged over spin-scattering channels) without and with Debye screening to the m-independent dynamically screened Born approximation with cutoff using two different ion-dynamics models. The theoretical values include Gaussian instrumental broadening of $\lambda/\Delta\lambda = 30\,390$.

			FWHM (Å)				
n_e (10^{23} m^{-3})	T (10^4 K)	D (a_0)	Expt. [19]	Born FFM/MMM	T matrix[a] FFM/MMM	T matrix[b] FFM/MMM	Simulation [38]
1	1.27	456	0.23 ± 0.02	0.16/0.19	0.17/0.21	0.17/0.20	0.22
2	1.32	335	0.30 ± 0.02	0.19/0.25	0.23/0.29	0.22/0.28	0.29
3	1.32	273	0.36 ± 0.02	0.23/0.29	0.30/0.37	0.28/0.35	0.36
4	1.40	243	0.42 ± 0.02	0.26/0.34	0.37/0.45	0.34/0.42	0.43

[a]Without Debye screening.
[b]With Debye screening for mean $D = 314a_0$.

IV. HYDROGENLIKE LITHIUM

For Li^{2+}, the Lyman series is studied for $T = 3 \times 10^5$ K and free-electron density $n_e = 4 \times 10^{25}$ m^{-3}, following the experimental conditions obtained in a laser-induced plasma experiment by Schriever *et al.* [39] and its analysis via synthetic spectral lines [40]. The corresponding Debye length is $D = 113a_0$. As the effect of strong collisions is more prominent for high densities, we consider the line profiles for a higher density $n_e = 4 \times 10^{26}$ m^{-3} as well.

The T-matrix approach is used without implementing the screening into the CCC code for the charged emitter Li^{2+}. Instead, we use scattering amplitudes from electron scattering on an isolated Li^{2+} ion. Since the long-range Coulomb potential gives rise to a divergent forward scattering amplitude, we skip the Coulomb part of the scattering amplitude. This does not affect the line profile operator because divergent terms in the self-energies are canceled by divergent terms in the coupling term; see Appendix A. An estimation of the necessary correction due to screening in the scattering process is given in Appendix B. The scattering amplitudes were calculated for $l = 60$ partial waves with an extrapolation to $l_{\max} = 125$.

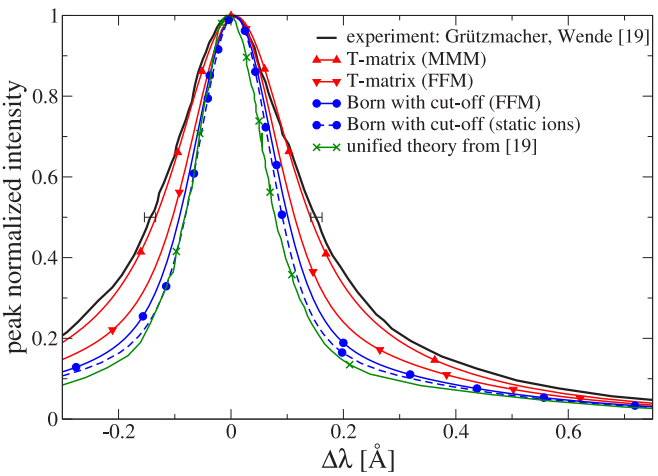

FIG. 3. (Color online) Comparison of measured and theoretical full H L_α profiles. Experimental data and unified theory are from Ref. [19] for plasma conditions $n_e = 2 \times 10^{23}$ m^{-3} and $T = 13\,200$ K. In the quantum-statistical theory, electrons are treated either in Born approximation with cutoff or within our T-matrix approach for $D = 314a_0$.

In Fig. 4, the Lyman lines are shown in Born approximation using Eqs. (8) and (9) with cutoff according to Eq. (10), and in the effective T-matrix approach Eqs. (12) and (13). We show the results averaged over the spin-scattering channels, as the differences in the resulting lines for the singlet and triplet channels are small. To focus on the effect of the different treatment of electrons, we neglect self-absorption and instrumental broadening in our comparison.

At the lower density (upper panel of Fig. 4), the screening correction for the T-matrix approach does not affect the line shape. In contrast to the comparison for H L_α, Fig. 2, the Li^{2+} L_α line is slightly redshifted when the T-matrix approach is used. For L_β and L_γ, the line shape is changed more drastically compared to the Born approximation result, leading to different asymmetric line features. The difference in the asymmetry is partly due to the different values for the self-energies in the two approximations. However, the main effect is again caused by the dependence on the magnetic quantum number m which is present only in the T-matrix approach. When Gaussian instrumental broadening with $\lambda/\Delta\lambda = 300$ [39] is applied, the prominent differences between the two approaches disappear. Thus, the analysis of the experiment would give the same results as previously presented in [40] and is not repeated here. It would be useful to have measurements with a better resolution for Li^{2+} to distinguish between the different theories.

At the higher density (lower panel of Fig. 4), the T-matrix approach gives a larger width compared to the Born approach. For L_α, the difference in the shift is equally pronounced and cannot be corrected by our simple screening correction. For L_β and even more for L_γ, the difference between the two approaches can be corrected to a large extent by the screening correction.

After these examples of full line profiles, we further study the influence of the screening correction in the T-matrix approach. For this reason, we give a comparison of the density dependence of the FWHM of L_α and L_β in Figs. 5 and 6 for a density range $n_e = 10^{25}$–2×10^{27} m^{-3} at $T = 3 \times 10^5$ K. For Li^{2+} L_α, the width is dominated by Doppler broadening up to $n_e = 10^{26}$ m^{-3}. For higher densities, the T-matrix approach gives a larger width even after applying

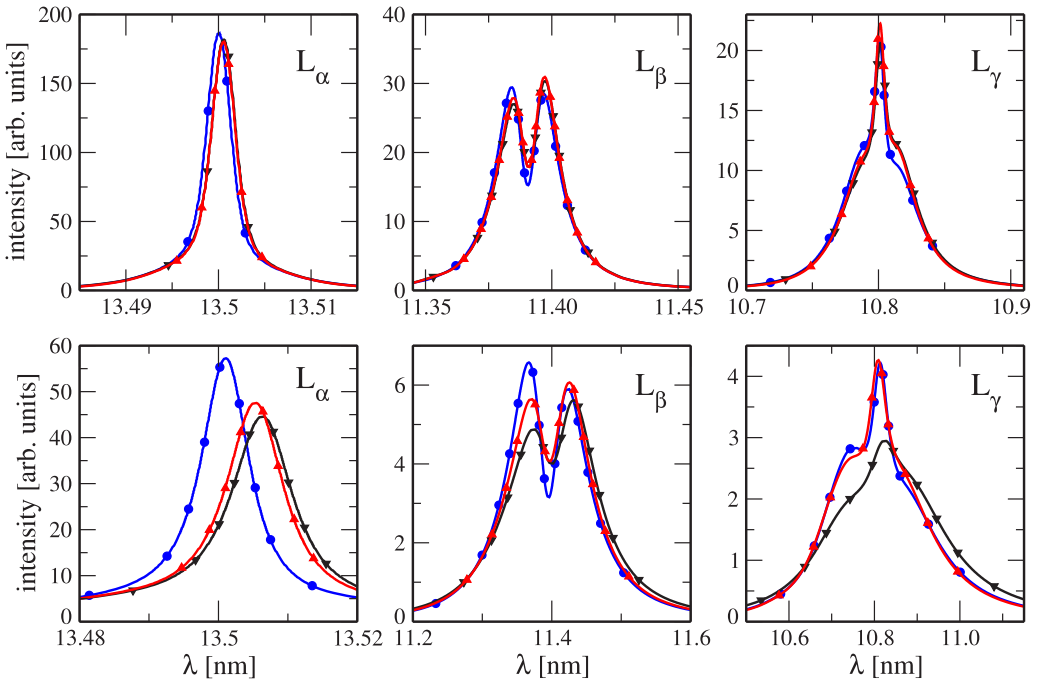

FIG. 4. (Color online) Area-normalized Lyman lines of Li^{2+} for $T = 3 \times 10^5$ K and $n_e = 4 \times 10^{25}$ m^{-3} (upper panel) and $n_e = 4 \times 10^{26}$ m^{-3} (lower panel), respectively. Electronic effects are treated in the dynamically screened Born approximation with cutoff (●) and with the T-matrix approach without screening (▼) and with an estimated screening correction (▲), according to Appendix B. Ion dynamics is considered within the FFM. Doppler broadening is included.

the screening correction. This might be due to the dependence on the magnetic quantum number m as discussed for H L_α in Sec. III A. For L_β, the screening correction leads to agreement of the FWHM from the T-matrix approach and that from the Born approach with cutoff.

For both considered one-electron emitters (H and Li^{2+}), the results of the perturbative Born approximation with adjusted cutoff are confirmed by our T-matrix approach for lower densities; see Figs. 3 and 4 (upper panel). There, the effect of strong collisions is expected to be small. For higher densities, and hence more strong collisions, differences between boththe two approaches are more pronounced; see Figs. 2 and 4 (lower panel). For the charged emitter Li^{2+}, plasma screening has not been implemented so far; however, our estimated correction leads to similar line shapes for both approaches. Remaining differences are caused by the different treatment of the dependence on the magnetic quantum number m. The screening of the charged emitter should be taken into account in the calculation of scattering amplitudes in the future.

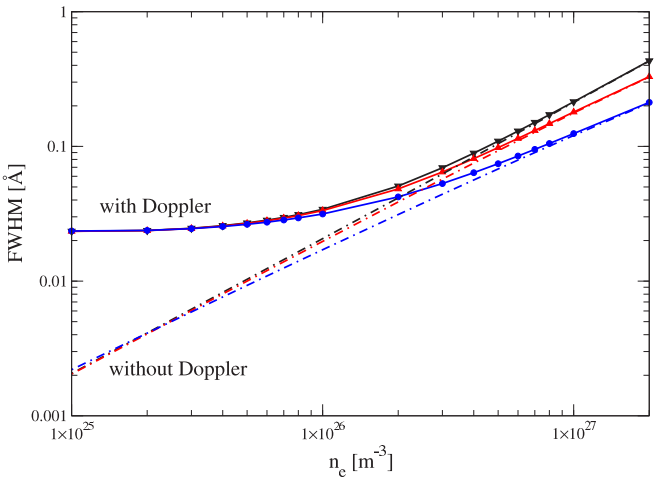

FIG. 5. (Color online) FWHM of Li^{2+} L_α line at $T = 3 \times 10^5$ K without ion dynamics. Electronic effects are treated in the dynamically screened Born approximation with cutoff (●) and in the T-matrix approach without screening (▼) and with an estimated screening correction (▲), according to Appendix B.

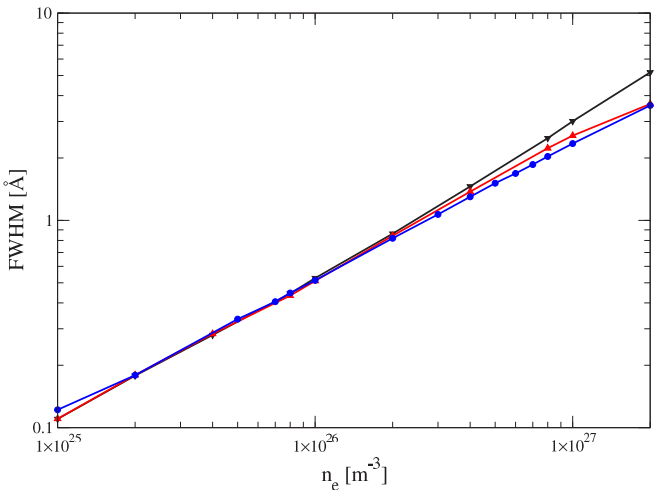

FIG. 6. (Color online) FWHM of Li^{2+} L_β line at $T = 3 \times 10^5$ K without ion dynamics. Legends are the same as in Fig. 5. Doppler broadening is included.

V. HELIUM 2 ^3S–3 ^3P

The quantum-statistical theory, originally developed for one-electron emitters, has also been extended to treat two-electron emitters; see Refs. [25,41,42]. There, an extensive comparison of the theory with measured data and results of other approaches has been given for several visible He lines. In this paper, we focus on the particular transition $2\,^3S$–$3\,^3P$, i.e., the He 3889 Å line. So far [41], the electronic self-energy had been considered only in the Born approximation within the cutoff procedure. In our calculations, we apply the effective two-particle T-matrix approach, Eq. (12), and consider strong collisions consistently. Furthermore, we take ion dynamics into account and apply the FFM from Eq. (5).

In Fig. 7, the theoretical FWHM and peak shifts of the He 3889 Å line are given as functions of the free-electron density. The results from our approach calculated in various approximations are compared to other theoretical data. In the T-matrix approach, ions are treated either quasistatically or dynamically within the FFM. Within the Born approach from Eq. (8), the inverse dielectric function consistently takes dynamical screening into account. The binary approximation ($\mathrm{Im}\,\varepsilon^{-1} \approx -\mathrm{Im}\,\varepsilon$) is also considered. Furthermore, nonquenching results are given, i.e., the sum in Eq. (8) includes only states of the same principal quantum number ($n_\alpha = n_\nu$). The different approximations were discussed in an earlier paper [41]. Our results are compared with molecular dynamics simulations [43,44] and Griem's standard theory [3]. The values for the latter are taken from Ref. [45].

The MD simulations of Gigosos *et al.* [43,44] were performed in density and temperature ranges of $n_e = (0.25\text{–}50) \times 10^{22}$ m^{-3} and $T = (2\text{–}6) \times 10^4$ K, respectively, in the nonquenching approximation for independent and interacting particles, respectively. Considering independent particles, they move along straight line trajectories at a constant speed. The correlation between the particles is considered only through the Debye-screened Coulomb interaction with the emitter. For interacting particles, all charge-charge coupling is considered. An ion-electron regularized Coulomb potential is chosen to account for quantum diffraction mechanisms in close collisions via the electron de Broglie wavelength. The correlation between perturbers tends to decrease the line broadening parameters at high electron densities [44]; see Fig. 7.

The width calculated in the T-matrix approach shows good agreement with the other theories, especially with the MD simulation data of Gigosos *et al.* [43] at high densities. The ion dynamics changes the linewidth only a little.

Compared to the MD simulation [43], the shift from the effective T-matrix approach is drastically reduced at lower densities. At $n_e = 9.8 \times 10^{22}$ m^{-3}, the shift agrees with Ref. [43]; see Fig. 7. At the highest densities, the line with the T-matrix approach is more shifted than the simulated one and reaches the nonquenching results of the Born approximation. The shift is generally overestimated in the Born approximation compared to our present results and the MD simulations. In contrast to the width, the shift is affected by the ion dynamics. Within the FFM, the shift is increased at lower densities compared to the quasistatic treatment.

In Fig. 8, we present the density dependence of the FWHM and peak shifts of the He 3889 Å line in comparison with measurements [45–52]. The Stark broadening parameters of this line are obtained by using the T-matrix approach with quasistatic ions and ion dynamics in the FFM, respectively. Furthermore, Doppler broadening is taken into account as well in Fig. 8.

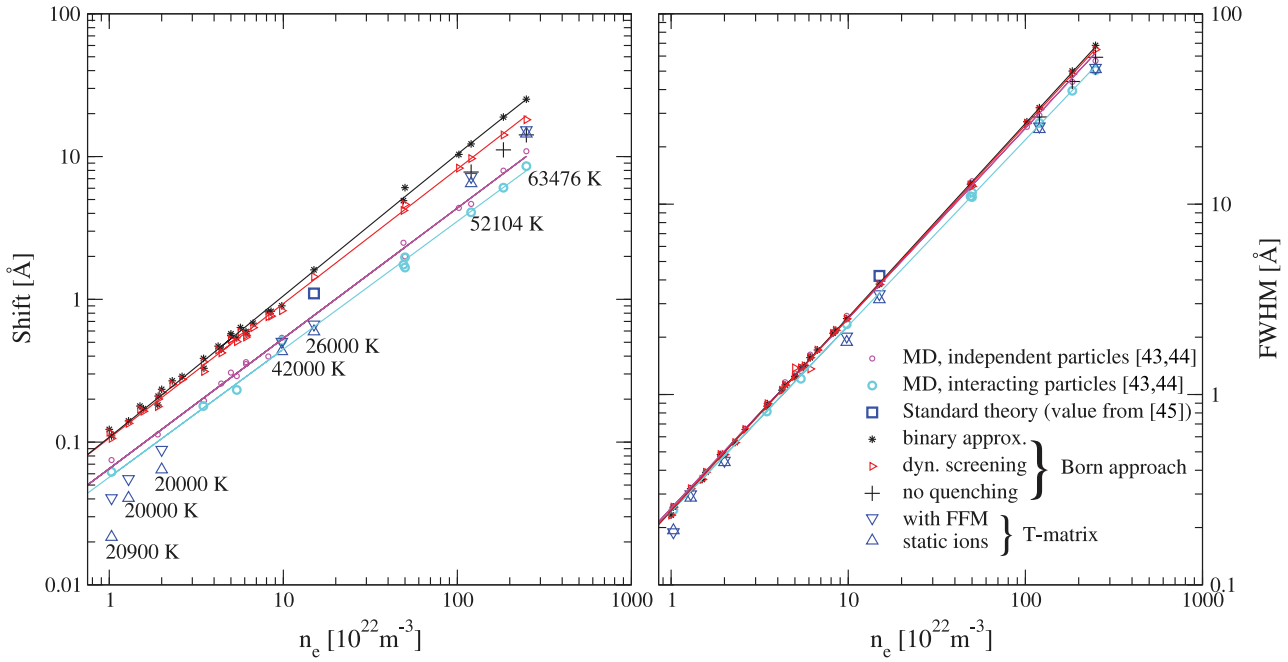

FIG. 7. (Color online) Shift and width of neutral He line 3889 Å vs electron density. The T-matrix approach with quasistatic ions and with ion dynamics in the FFM is compared to the Born approach in different approximations and to results from MD simulations [43,44] and from Griem's standard theory [3,45]. The electron temperature is given for the T-matrix data points (left).

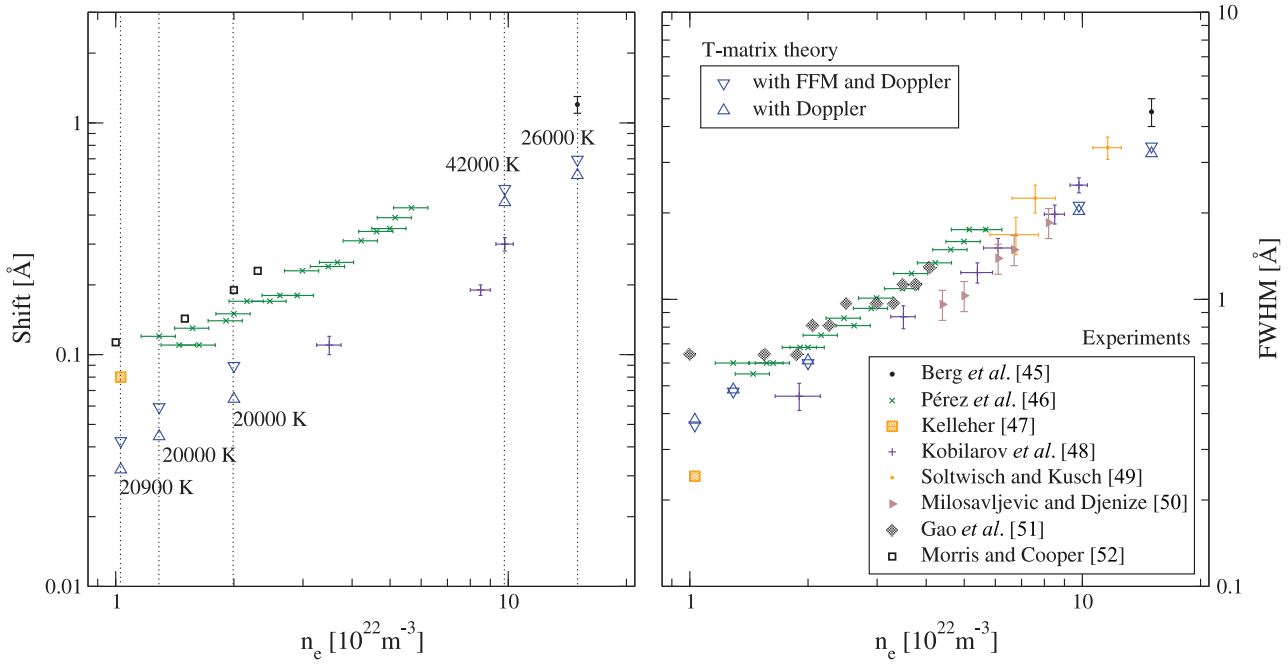

FIG. 8. (Color online) Shift and FWHM of neutral He line at 3889 Å vs electron density. The T-matrix approach with quasistatic ions and with ion dynamics in the FFM including Doppler broadening is compared to measured data [45–52].

The following experiments are included in Fig. 8: The measurement by Pérez *et al.* [46] was made in a plasma of a low-pressure pulsed arc, within the plasma density range of $n_e = (1\text{–}6) \times 10^{22}$ m^{-3} and temperature interval of $T = (0.8\text{–}3) \times 10^4$ K with a mean value of 2×10^4 K. The error bar of n_e was ±10%, and the uncertainty in the temperature evaluation was about 20%. The experimental result of Kelleher [47] was obtained in a helium plasma generated in a wall-stabilized arc, with $n_e = 1.03 \times 10^{22}$ m^{-3} and $T_e = 2.09 \times 10^4$ K. Recently, the FWHM of the same transition line was measured by Gao *et al.* [51] from a helium arc for the density range $n_e = (0.5\text{–}4) \times 10^{22}$ m^{-3} at $T = 2.3 \times 10^4$ K. Values reported by Kobilarov *et al.* [48] from a pulsed low-pressure arc at $n_e = (2\text{–}10) \times 10^{22}$ m^{-3} and $T = (3.1\text{–}4.2) \times 10^4$ K are included. Note that the shift at the half-width is given in this case. Furthermore, values for the shift measured by Morris and Cooper [52] within the density range $n_e = (0.6\text{–}2.3) \times 10^{22}$ m^{-3} and temperature $T = (1\text{–}1.6) \times 10^4$ K are shown. The Stark parameters of this line were also measured by Berg *et al.* [45] at $n_e = 1.5 \times 10^{22}$ m^{-3} and $T = 2.6 \times 10^4$ K. The measured values by Milosavljević and Djeniže [50] at $n_e = (4.4\text{–}8.2) \times 10^{22}$ m^{-3} and at $T = (1.8\text{–}3.3) \times 10^4$ K by using a linear low-pressure pulsed arc are given as well.

In Table III, a numerical comparison of the FWHM from the T-matrix approach to the corresponding experimental data [45–48] is given. Ion dynamics (FFM) and Doppler broadening are included in the T-matrix results. Furthermore, the FWHM results from the Born approximation with dynamical screening are included as well as the result of MD simulations for interacting particles [43]. Since the ion dynamics affect the width only slightly (see Fig. 7), we can directly compare the width in the Born approximation within quasistatic ion motion with the one from our T-matrix approach. As shown in Fig. 7, the T-matrix approach always gives a smaller FWHM than the Born approximation. This trend leads to a better agreement with the experiment at the lowest density, i.e., for the FWHM of Kelleher [47]. For the data of Pérez *et al.* [46], the calculated width in the T-matrix approach with and without Doppler broadening agrees very well with the result of the Born approximation. However, the measured FWHM is higher than the calculated one; this may be due to self-absorption, as mentioned in Ref. [46]. At $n_e = 9.8 \times 10^{22}$ m^{-3}, our results in the Born approximation show a very good agreement with both measurement and MD simulation data. However, the T-matrix

TABLE III. Theoretical calculations of the FWHM of the He 3889 Å line from the T-matrix approach and the Born approximation are compared with measurements and MD simulations [43]. The FWHM is given in Å.

n_e	T_e	FWHM (Å)			
(10^{22} m^{-3})	(10^4 K)	Expt.	[43][a]	T matrix[b]	Born[c]
1.03 ± 0.12	2.1 ± 0.2	0.24[d]	0.25	0.30/0.19	0.34/0.25
1.29 ± 0.10	2.0 ± 0.2	0.6[e]		0.40/0.30	0.41/0.31
2.00 ± 0.10	2.0 ± 0.2	0.68[e]		0.53/0.45	0.55/0.47
9.8 ± 0.5	4.2	2.5 ± 0.15[f]	2.34	2.06/2.02	2.48/2.45
15.0 ± 0.8	2.6 ± 0.2	4.5 ± 0.5[g]		3.39/3.37	3.76/3.75

[a]Molecular dynamics simulations with interacting particles, without Doppler broadening.
[b]T-matrix approach (FFM ion dynamics, with/without Doppler broadening).
[c]Dynamical screening, with/without Doppler broadening.
[d]Kelleher [47].
[e]Pérez *et al.* [46].
[f]Kobilarov *et al.* [48].
[g]Berg *et al.* [45].

approach gives a lower value outside the validity range given in the experiment. At the highest measured density, the FWHM of both theories is below that of Berg *et al*. [45]. Note that the contribution of Doppler broadening to the linewidth is reduced with increasing density, i.e., with increasing Stark broadening.

VI. CONCLUSION

We use a quantum-statistical approach to calculate full line profiles of neutral emitters (H, He) and a charged H-like emitter (Li^{2+}). To go beyond the Born approximation, we apply a T-matrix approach based on scattering amplitudes for plasma pressure broadening caused by electrons. Thus, strong electron-emitter collisions are included implicitly. Scattering amplitudes are calculated within a sophisticated close-coupling scheme, taking static plasma screening into account for neutral emitters.

For H L_α, we analyze the effect of screening on the scattering amplitudes. They are reduced by screening, thus leading to narrower and less shifted lines. For the linewidth, we could verify the validity of the cutoff procedure, which is implemented in the Born approximation to compensate the overestimation of strong collisions. However, the shift is still overestimated when using the cutoff procedure adjusted to an advanced T-matrix calculation [33]. Furthermore, the line shape differs due to the dependence on the magnetic quantum number m in the effective two-particle T-matrix approach. Finally, we reconsidered the experiment of Grützmacher and Wende [19]. There, the T-matrix approach leads to a satisfying agreement with the experiment. However, the resulting linewidth depends strongly on the ion-dynamics theory considered.

For Li^{2+}, the Lyman lines were calculated for the experimental conditions of Schriever *et al*. [39]. Small differences in the details of the line shape can be found between the Born and the T-matrix approaches. However, they disappear as soon as Gaussian instrumental broadening is applied. Thus, our calculation confirms the previous analysis of Ref. [40], which was based only on the Born approach. The density dependence of the width was here studied in more detail, taking into account an estimated screening correction. The unscreened T-matrix approach generally leads to broader linewidths than the Born approach with a cutoff. The screening correction reduces the difference in the width drastically.

For the He I line at 3889 Å, the FWHM and shift are compared with results of other theories and several experiments for a broad range of densities. The shift is overestimated in the Born approximation even after adopting the cutoff procedure to account for strong electron-emitter collisions. On the other hand, underestimation can be seen for the T-matrix approach compared to the MD simulation data. However, the FWHM values from both theoretical approaches are in good agreement with each other and with the MD simulation data. Further, the effect of ion dynamics is pronounced at lower electron densities, especially for the shift of the line. The discrepancy between the measured and calculated line broadening is partially related to self-absorption [51].

Thus, we showed that the effective two-particle T-matrix approach gives the possibility to treat strong electron-emitter collisions in a consistent way. Plasma screening was treated with static Debye theory in the case of neutral emitters, and approximated in the case of charged emitters. It would be important to extend the approach to include dynamic screening. Thus, the proper treatment of the plasma screening has to be investigated in the future.

Ion dynamics has not been discussed in detail in this work. Since we have not implemented the model microfield method for He and Li^{2+} yet, we were restricted to the use of the frequency-fluctuation model. However, we note that our calculations for H in comparison to the Grützmacher-Wende profiles suggest the MMM as the better choice for ion-dynamics calculations. Hence, further investigations of ion dynamics are necessary. Furthermore, for the analysis of laser-produced plasmas, like the one presented in [39], an extension to nonequilibrium physics is crucial.

ACKNOWLEDGMENTS

We would like to thank Heidi Reinholz and Gerd Röpke for their advice, Sandrine Ferri for suggesting use of the FFM, and Joël Rosato for the discussion of correlated collisions. This work was supported by the German Research Foundation DFG within SFB 652. The support of the Australian Research Council, the Australian National Computational Infrastructure Facility, and its Western Australian node iVEC are gratefully acknowledged.

APPENDIX A: SPLITTING OF INTERNAL AND EXTERNAL PARTS OF THE SCATTERING AMPLITUDE

To handle the divergent Coulomb part of the scattering amplitude, we split the total scattering phases

$$\delta_l^{C+\mathrm{in}} = \delta_l^C + \delta_l^{\mathrm{in}}, \tag{A1}$$

into an inner part δ_l^{in} which depends on the excitation state and the atomic structure of the emitter and an outer part δ_l^C which is independent of the emitter state. For the Li^{2+} example, δ_l^C is due to the long-ranging Coulomb potential with $Z = 2$.

The scattering amplitudes for electron scattering at the initial and final emitter states are given by

$$f_i(\theta,k) = \frac{1}{2\imath k}\sum_{l=0}^{\infty}(2l+1)\left(e^{2\imath(\delta_l^C+\delta_{l,i}^{\mathrm{in}})}-1\right)P_l[\cos(\theta)], \tag{A2}$$

$$f_f(\theta,k) = \frac{1}{2\imath k}\sum_{l=0}^{\infty}(2l+1)\left(e^{2\imath(\delta_l^C+\delta_{l,f}^{\mathrm{in}})}-1\right)P_l[\cos(\theta)], \tag{A3}$$

with the Legendre polonomials $P_l[x]$.

For the forward scattering, the scattering amplitude can be constructed from its parts. Here, we neglect the k dependence for the sake of clarity. We start with the following expression:

$$\begin{aligned}\int_0^\pi d\theta\,\sin(\theta) f^C(\theta) f^{\mathrm{in}}(\theta) &= \sum_{ll'}(2l+1)(2l'+1)\left(\frac{1}{2\imath k}\right)^2\left\{\left(e^{2\imath\delta_l^C}-1\right)\left(e^{2\imath\delta_{l'}^{\mathrm{in}}}-1\right)\right\}\\ &\quad\times\int_0^\pi d\theta\,\sin(\theta)P_l[\cos(\theta)]P_{l'}[\cos(\theta)].\end{aligned} \tag{A4}$$

With two simplifications

$$\int_0^\pi d\theta \sin(\theta) P_l[\cos(\theta)] P_{l'}[\cos(\theta)] = \frac{2}{2l+1}\delta_{ll'}, \tag{A5}$$

$$\begin{aligned}\{\cdots\} &= e^{2\imath(\delta_l^C+\delta_l^{\rm in})} - e^{2\imath\delta_l^C} - e^{2\imath\delta_l^{\rm in}} + 1 + (1-1)\\ &= \left(e^{2\imath(\delta_l^C+\delta_l^{\rm in})} - 1\right) - \left(e^{2\imath\delta_l^C} - 1\right) - \left(e^{2\imath\delta_l^{\rm in}} - 1\right),\end{aligned} \tag{A6}$$

we obtain

$$\begin{aligned}&\int_0^\pi d\theta \sin(\theta) f^C(\theta) f^{\rm in}(\theta)\\ &\quad = \frac{1}{\imath k}\{f^{\rm C+in}(0) - f^{\rm C}(0) - f^{\rm in}(0)\}.\end{aligned} \tag{A7}$$

And thus,

$$f^{C+{\rm in}}(0) = f^C(0) + f^{\rm in}(0) + \imath k \int_0^\pi d\theta \sin(\theta) f^C(\theta) f^{\rm in}(\theta), \tag{A8}$$

and analogously, for the complex conjugate

$$\begin{aligned}f^{C+{\rm in}*}(0) &= f^{C*}(0) + f^{{\rm in}*}(0)\\ &\quad - \imath k \int_0^\pi d\theta \sin(\theta) f^{C^*}(\theta) f^{{\rm in}*}(\theta).\end{aligned} \tag{A9}$$

However, for the coupling term, we need the full θ dependence of $f_i(\theta,k)$ and $f_f(\theta,k)$. In the vertex term, we have (again dropping the k dependence)

$$\begin{aligned}\imath \int_0^\pi d\theta \sin(\theta) f_i^*(\theta) f_f(\theta) = \imath \int_0^\pi d\theta \sin(\theta) \Bigg\{ &\frac{-1}{2\imath k}\sum_{l=0}^\infty (2l+1)\left(e^{-2\imath(\delta_l^C+\delta_{l,i}^{\rm in})} - 1\right) P_l[\cos(\theta)]\\ &\times \frac{1}{2\imath k}\sum_{l'=0}^\infty (2l'+1)\left(e^{2\imath(\delta_{l'}^C+\delta_{l',f}^{\rm in})} - 1\right) P_{l'}[\cos(\theta)]\Bigg\}.\end{aligned} \tag{A10}$$

Using again the orthogonality of Legendre polynomials, we obtain

$$\imath \int_0^\pi d\theta \sin(\theta) f_i^*(\theta) f_f(\theta) = \frac{\imath}{2k^2}\sum_{l=0}^\infty (2l+1)\left\{\left(e^{-2\imath(\delta_l^C+\delta_{l,i}^{\rm in})} - 1\right)\left(e^{2\imath(\delta_l^C+\delta_{l,f}^{\rm in})} - 1\right)\right\}. \tag{A11}$$

The coupling term of the inner structure alone is given by

$$\begin{aligned}\imath \int_0^\pi d\theta \sin(\theta) f_i^{{\rm in}*}(\theta) f_f^{\rm in}(\theta) &= \imath \int_0^\pi d\theta \sin(\theta) \Bigg\{ \frac{-1}{2\imath k}\sum_{l=0}^\infty (2l+1)\left(e^{-2\imath(\delta_{l,i}^{\rm in})} - 1\right) P_l[\cos(\theta)]\\ &\quad \times \frac{1}{2\imath k}\sum_{l'=0}^\infty (2l'+1)\left(e^{2\imath(\delta_{l',f}^{\rm in})} - 1\right) P_{l'}[\cos(\theta)]\Bigg\}\end{aligned} \tag{A12}$$

$$= \frac{\imath}{2k^2}\sum_{l=0}^\infty (2l+1)\left\{e^{2\imath(\delta_{l,f}^{\rm in}-\delta_{l,i}^{\rm in})} - e^{2\imath\delta_{l,f}^{\rm in}} - e^{-2\imath\delta_{l,i}^{\rm in}} + 1\right\}. \tag{A13}$$

Expanding the term in the braces in Eq. (A11) and adding missing terms to obtain the inner coupling term, we obtain for the full coupling term

$$\imath \int_0^\pi d\theta \sin(\theta) f_i^*(\theta) f_f(\theta) = \imath \int_0^\pi d\theta \sin(\theta) f_i^{{\rm in}*}(\theta) f_f^{\rm in}(\theta) + \frac{\imath}{2k^2}\sum_{l=0}^\infty (2l+1)\left\{ - e^{2\imath(-\delta_l^C-\delta_{l,i}^{\rm in})} - e^{2\imath(\delta_l^C+\delta_{l,f}^{\rm in})} + e^{2\imath\delta_{l,f}^{\rm in}} + e^{-2\imath\delta_{l,f}^{\rm in}}\right\}. \tag{A14}$$

The first term is the vertex term for the inner structure alone, the second term can be rearranged as

$$\frac{\imath}{2k^2}\sum_{l=0}^\infty (2l+1)\left\{ - e^{2\imath(-\delta_l^C-\delta_{l,i}^{\rm in})} - e^{2\imath(\delta_l^C+\delta_{l,f}^{\rm in})} - e^{2\imath\delta_{l,f}^{\rm in}} - e^{-2\imath\delta_{l,f}^{\rm in}}\right\} \tag{A15}$$

$$= -\frac{\imath}{2k^2}\sum_{l=0}^\infty (2l+1)\left\{\left(e^{2\imath\delta_{l,f}^{\rm in}} - 1 + 1\right)\left(e^{2\imath(\delta_l^C)} - 1\right) + \left(e^{-2\imath\delta_{l,f}^{\rm in}} - 1 + 1\right)\left(e^{-2\imath(\delta_l^C)} - 1\right)\right\} \tag{A16}$$

$$\begin{aligned}&= \frac{\imath}{4\imath^2 k^2}\sum_{ll'} (2l+1)(2l'+1)\left\{\left(e^{2\imath\delta_{l',f}^{\rm in}} - 1\right)\left(e^{2\imath(\delta_l^C)} - 1\right) + \left(e^{-2\imath\delta_{l',f}^{\rm in}} - 1\right)\left(e^{-2\imath(\delta_l^C)} - 1\right)\right\}\\ &\quad \times \int_0^\pi d\theta \sin(\theta) P_l[\cos(\theta)] P_{l'}[\cos(\theta)] + \frac{1}{k} f^C(0) - \frac{1}{k} f^{C*}(0)\end{aligned} \tag{A17}$$

$$= \imath \int_0^\pi d\theta \sin(\theta)\left\{ f_f^{\rm in}(\theta) f^C(\theta) + f_i^{{\rm in}*}(\theta) f^{C*}(\theta)\right\} + \frac{1}{k} f^C(0) - \frac{1}{k} f^{C*}(0). \tag{A18}$$

With this expression, we can consider the full line profile operator as in Eq. (3). With the electronic contributions to the self-energy Eq. (12) and the coupling term Eq. (13) we have

$$L(\Delta\omega,E) = \Delta\omega - \mathrm{Re}[\Sigma_i - \Sigma_f] + \imath\,\mathrm{Im}[\Sigma_i + \Sigma_f] + \Gamma_{ii'ff'} \tag{A19}$$

$$= \Delta\omega + \Sigma_f - \Sigma_i^* + \Gamma_{ii'ff'} \tag{A20}$$

$$= \Delta\omega + A\left(f_f^{C+\mathrm{in}}(0,k) - f_i^{C+\mathrm{in}*}(0,k) - \imath k \int_0^\pi d\theta\, \sin(\theta) f_i^{C+\mathrm{in}*}(\theta) f_f^{C+\mathrm{in}}(\theta) \right). \tag{A21}$$

Here, the function $A(x(k))$ was introduced consisting of the prefactor and the k integration,

$$A(x(k)) = -\frac{2}{\pi} n_e \Lambda_{\mathrm{th}}^3 \int_0^\infty dk\, k^2 e^{-k^2/k_B T} x(k). \tag{A22}$$

The argument of this function is

$$x(k) = f_f^{C+\mathrm{in}}(0,k) - f_i^{C+\mathrm{in}*}(0,k) - \imath k \int_0^\pi d\theta\, \sin(\theta) f_i^{C+\mathrm{in}*}(\theta) f_f^{C+\mathrm{in}}(\theta). \tag{A23}$$

Using Eqs. (A8), (A9), and (A18), we obtain

$$x(k) = f_f^{\mathrm{in}}(0) - f_i^{\mathrm{in}*}(0) - \imath k \int_0^\pi d\theta\, \sin(\theta) f_f^{\mathrm{in}}(\theta) f_i^{\mathrm{in}*}(\theta). \tag{A24}$$

This is exactly the result one would obtain by neglecting δ_C. Thus, the divergent Coulomb terms in the self-energies are canceled by the ones in the coupling term and it is legitimate to neglect them in the calculation.

APPENDIX B: ESTIMATION OF ERROR MADE BY NEGLECTING SCREENING IN e-Li^{2+} SCATTERING

Following the reasoning in Appendix A, the fact that the long-range ($Z = 2$) potential is screened does not change the line shape when considering binary collisions. However, the screening within the atom and the resulting change of the inner structure do affect the scattering process and, thus, the line shape. To obtain a measure for the change of the inner structure, we consider first the Debye shift [53] relative to the energy of a level with quantum number n,

$$X(D,n,Z) = \frac{\Delta E}{E_n} = \frac{\frac{2Z}{D}}{\frac{Z^2}{n^2}} = \frac{2n^2}{ZD}. \tag{B1}$$

TABLE IV. Relative change in % of electronic width and shift from the unscreened to the screened calculation of H($2p$, $m = \pm 1$) with coupling to H($1s$) for different temperatures.

	$D = 314a_0$, $X = 2.55\%$					$D = 44a_0$, $X = 18.2\%$				
k_BT (eV)	1	2	10	20	26	1	2	10	20	26
Width	−11	−9.3	−5.5	−3.7	−3.0	−58	−52	−35	−28	−25
Shift	−22	−16	−5.8	−3.9	−3.5	−63	−62	−47	−41	−40

TABLE V. Relative Debye shift X and relative error estimates in % for the electronic contribution to the shift and width of the Lyman lines of Li^{2+} at $T = 3 \times 10^5$ K, as shown in Fig. 4.

	$D = 113a_0$			$D = 35a_0$		
	L_α	L_β	L_γ	L_α	L_β	L_γ
X (%)	2.4	5.3	9.4	7.6	17.1	30.5
Width	−3	−7	−13	−10	−24	−42
Shift	−4	−10	−20	−15	−37	−67

This gives us a connection between our hydrogen calculations ($Z = 1$) and any H-like emitter. We calculated the H L_α line with unscreened and screened scattering amplitudes ($D = \infty$, $D = 314a_0$, $D = 44a_0$). In Table IV, we compare the relative change of width and shift of the central component of the L_α line for several temperatures. It can be seen that the effect decreases with temperature. This can be understood from Fig. 1, which shows that screening changes the scattering amplitudes especially for small k values. Higher temperatures shift the Boltzmann distribution in Eqs. (12) and (13) to higher k values and thus to regions which are less affected by the screening. We include the values for $T = 3 \times 10^5$ K, i.e., for 26 eV as this is the temperature in our Li^{2+} example.

For $D = 314a_0$ and $D = 44a_0$, the relative Debye shifts of the $n = 2$ level are $X(314,2,1) = 2.55\%$ and $X(44,2,1) = 18.2\%$, respectively. The X values for the Li^{2+} Lyman lines from Fig. 4 are given in Table V together with an estimate of the relative correction due to screening in the scattering process. The estimate is based on the assumption that the effect on the electronic part of the line shape is similar for the same value of X for different emitters at a certain temperature, using an interpolation linear in X.

In Fig. 9, the screening correction is shown for Li^{2+} L_α, L_β, and L_γ lines for a broad density range.

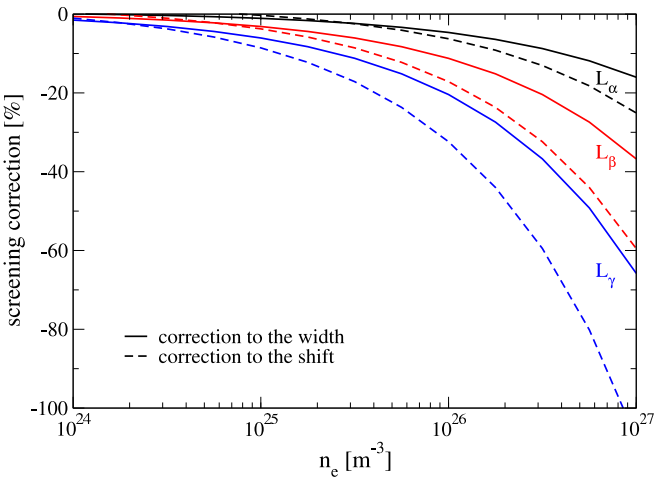

FIG. 9. (Color online) Relative correction to the electronic width and shift of Lyman lines of Li^{2+} due to screening. Calculated for $T = 3 \times 10^5$ K.

[1] H. R. Griem, *Principles of Plasma Spectroscopy* (Cambridge University Press, Cambridge, 1997).
[2] M. Baranger, Phys. Rev. **112**, 855 (1958).
[3] H. R. Griem, *Spectral Line Broadening by Plasmas* (Academic Press, London, 1974).
[4] S. Sahal-Brechot, Astron. Astrophys. **1**, 91 (1969); **2**, 322 (1969).
[5] R. Stamm and D. Voslamber, J. Quant. Spectrosc. Radiat. Transfer **22**, 599 (1979).
[6] L. Hitzschke, G. Röpke, T. Seifert, and R. Zimmermann, J. Phys. B **19**, 2443 (1986).
[7] S. Günter, Habilitation thesis, Rostock University, Germany, 1995.
[8] S. Sorge, A. Wierling, G. Röpke, W. Theobald, R. Sauerbrey, and T. Wilhein, J. Phys. B **33**, 2983 (2000).
[9] S. Alexiou and A. Poquerusse, Phys. Rev. E **72**, 046404 (2005).
[10] S. Lorenzen, A. Wierling, H. Reinholz, and G. Röpke, Contrib. Plasma Phys. **51**, 349 (2011).
[11] M. C. Zammit, D. V. Fursa, and I. Bray, Phys. Rev. A **82**, 052705 (2010).
[12] M. C. Zammit, D. V. Fursa, I. Bray, and R. K. Janev, Phys. Rev. A **84**, 052705 (2011).
[13] K. Unnikrishnan and J. Callaway, Phys. Rev. A **43**, 3619 (1991).
[14] I. Bray and A. T. Stelbovics, Phys. Rev. A **46**, 6995 (1992).
[15] I. Bray and D. V. Fursa, J. Phys. B **44**, 061001 (2011).
[16] I. Bray, D. V. Fursa, A. S. Kadyrov, A. T. Stelbovics, A. S. Kheifets, and A. M. Mukhamedzhanov, Phys. Rep. **520**, 135 (2012).
[17] A. Calisti, C. Mossé, S. Ferri, B. Talin, F. Rosmej, L. A. Bureyeva, and V. S. Lisitsa, Phys. Rev. E **81**, 016406 (2010).
[18] E. Stambulchik, High Energy Density Phys. **9**, 528 (2013).
[19] K. Grützmacher and B. Wende, Phys. Rev. A **16**, 243 (1977).
[20] C. F. Hooper, Jr., Phys. Rev. **165**, 215 (1968); **169**, 193 (1968).
[21] A. Y. Potekhin, G. Chabrier, and D. Gilles, Phys. Rev. E **65**, 036412 (2002).
[22] C. A. Iglesias, Phys. Rev. A **27**, 2705 (1983).
[23] L. D. Landau and E. M. Lifschitz, *Quantum Mechanics: Non-Relativistic Theory* (Pergamon Press, Oxford, 1977).
[24] D. R. Bates and A. Damgaard, Philos. Trans. R. Soc., A **242**, 101 (1949).
[25] B. Omar, S. Günter, A. Wierling, and G. Röpke, Phys. Rev. E **73**, 056405 (2006).
[26] J. Halenka, Z. Phys. D **16**, 1 (1990).
[27] A. V. Demura, Int. J. Spectrosc **2010**, 671073 (2010).
[28] A. Brissaud and U. Frisch, J. Quant. Spectrosc. Radiat. Transfer **11**, 1767 (1971).
[29] J. Seidel, Z. Naturforsch. **32a**, 1195 (1977); **35a**, 679 (1980).
[30] S. Lorenzen, Contrib. Plasma Phys. **53**, 368 (2013).
[31] J. Rosato, H. Capes, and R. Stamm, Phys. Rev. E **86**, 046407 (2012).
[32] J. Rosato, H. Capes, and R. Stamm, High Energy Density Phys. **9**, 484 (2013).
[33] S. Günter, Phys. Rev. E **48**, 500 (1993).
[34] H. R. Griem, M. Baranger, A. C. Kolb, and G. Oertel, Phys. Rev. **125**, 177 (1962).
[35] S. Lorenzen, A. Wierling, H. Reinholz, G. Röpke, M. C. Zammit, D. V. Fursa, and I. Bray, in *Proceedings of the 20th International Conference on Spectral Line Shapes*, edited by J. Lewis and A. Predoi-Cross, AIP Conf. Proc. No. 1290 (AIP, New York, 2010), p. 99; J. Phys.: Conf. Ser. **397**, 012021 (2012).
[36] T. O'Malley, L. Spruch, and L. Rosenberg, J. Math. Phys. **2**, 491 (1961).
[37] R. W. Lee, J. Phys. B **11**, L167 (1978).
[38] J. Halenka and W. Olchawa, J. Quant. Spectrosc. Radiat. Transfer **56**, 17 (1996).
[39] G. Schriever, K. Bergmann, and R. Lebert, J. Appl. Phys. **83**, 4566 (1998).
[40] S. Lorenzen, A. Wierling, H. Reinholz, and G. Röpke, Contrib. Plasma Phys. **48**, 657 (2008).
[41] B. Omar, Int. J. Spectrosc. **2010**, 983578 (2010).
[42] B. Omar, A. Wierling, H. Reinholz, and G. Röpke, Phys. Rev. Res. Int. **3**, 218 (2013).
[43] M. A. Gigosos, M. A. Gonzalez, V. Talin, and A. Calisiti (unpublished).
[44] M. A. Gigosos, M. A. Gonzalez, V. Talin, and A. Calisiti, in *Proceedings of the 17th International Conference on Spectral Line Shapes*, edited by E. Dalimier (Frontier Group, Paris, 2004), p. 451.
[45] H. F. Berg, A. W. Ali, R. Lincke, and H. R. Griem, Phys. Rev. **125**, 199 (1962).
[46] C. Pérez, R. Santamarta, M. I. de la Rosa, and S. Mar, Eur. Phys. J. D **27**, 73 (2003).
[47] D. E. Kelleher, J. Quant. Spectrosc. Radiat. Transfer **25**, 191 (1981).
[48] R. Kobilarov, N. Konjević, and M. V. Popović, Phys. Rev. A **40**, 3871 (1989).
[49] H. Soltwisch and H. J. Kusch, Z. Naturforsch. **34a**, 300 (1979).
[50] V. Milosavljević and S. Djeniže, New Astron. **7**, 543 (2002).
[51] H. M. Gao, S. L. Ma, C. M. Xu, and L. Wu, Eur. Phys. J. D **47**, 191 (2008).
[52] R. N. Morris and J. Cooper, Can. J. Phys. **51**, 1746 (1973).
[53] H. R. Griem, Phys. Rev. **128**, 997 (1962).